ADVANCED OXIDATION/REDUCTION TECHNOLOGIES: AN PERSPECTIVE FROM IBEROAMERICAN COUNTRIES

Degradation of pharmaceuticals in wastewater matrices through solar light-driven photocatalyst prepared from petrochemical waste

Elisabeth Cuervo Lumbaque[1] · Cálita Elis Schweigert[1] · Leonardo Oliveira dos Santos[1] · Vladimir Lavayen[1] · João Henrique Zimnoch dos Santos[1] · Carla Sirtori[1]

Abstract

Pharmaceuticals, such as dipyrone (DIP), paracetamol (PCT), and propranolol (PPN), are widely used analgesics and beta-blockers with the greatest presence in wastewaters and, consequently, in natural waters. The present work evaluated solar light-driven photocatalyst from petrochemical industrial waste (PW) as a strategy for the degradation of three pharmaceuticals in different water matrices (distilled water-DW, simulated wastewater-SWW, and real hospital wastewater-RHWW). All experiments were carried out in a solar photo-reactor with a capacity of 1 L and the experimental condition employed was a catalyst concentration of 350 mg L^{-1} at pH 5.0; these conditions were selected considering the Doehlert design validation spreadsheet and the desirability function. All materials prepared were conveniently characterized by zeta potential, small-angle X-ray scattering (SAXS), diffuse reflectance ultraviolet-visible (DRUV), and infrared spectroscopy. According to the results of the characterization, significant differences have been observed between the PW and the photocatalyst such as vibrational modes, optical absorption gap, and acid-basic characteristics on the surface, which suggests the potential use of the photocatalyst in the degradation of contaminants of emerging concern. Based on pharmaceutical degradation, DIP showed the highest photosensitivity (87.5%), and therefore the highest photocatalytic degradation followed by PPN; both compounds achieved final concentrations below the limit of quantification of the chromatographic method in DW. However, PCT was the most recalcitrant pharmaceutical in all matrices. Radicals from chromophoric natural organic matter (NOM) could improve PCT degradation in the SWW matrix (56%). Nevertheless, the results in RHWW showed a matrix effect with decreased the oxidation percentages (DIP-99%; PPN-71%; PCT-17%); hence, the addition of an oxidant such as H_2O_2 was studied as a pharmaceutical oxidation boost in RHWW. PPN was the molecule most sensitive to this strategy of oxidation (98%). Furthermore, 20 transformation products (TPs) generated throughout the treatment were identified by LC-QTOF MS using a customized TPs database. According to quantitative structure activity relationship (Q)SAR analysis, more than 75% of the TPs identified were not

Highlights

- The potential use of the photocatalyst from petrochemical industry waste.
- Solar photocatalysis degrades high percentages of dipyrone and propranolol.
- 20 transformation products (TPs) were identified by LC-QTOF MS.
- TPs database associated with (Q)SAR tools as a toxicity assessment proposal.
- In (Q)SAR analysis, more than 75% of the TPs identified were not biodegradable.

✉ Carla Sirtori
  carla.sirtori@ufrgs.br

1   Instituto de Química—Universidade Federal do Rio Grande do Sul, Av. Bento Gonçalves, 9500, Porto Alegre, RS 91501 - 970, Brazil

biodegradable. About 35% of them have oral toxicity characteristics indicated by Cramer's rules, and the DIP TPs represent high toxicity for different trophic levels.
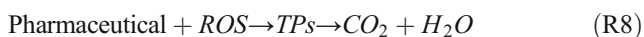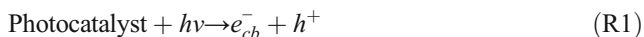
Introduction

In recent years, the consumption and manufacture of pharmaceutical products has grown worldwide, without legislation that controls their elimination and concentrations in wastewater; due to these, characteristics and toxicological potential are considered such as "contaminants of emerging concern (CECs)"(Chung and Brooks 2019). Recent studies have shown that analgesics and beta-blockers are the group of pharmaceuticals with the greatest presence in hospital wastewater and wastewater treatment plants (Santos et al. 2013; Čelić et al. 2019; Becker et al. 2020). The commonly used analgesics such as paracetamol (PCT) and dipyrone (DIP), as well as the beta-blocker propranolol (PPN), cannot be completely eliminated in sewage treatment and present toxicity to a wide variety of aquatic species (Pamplona et al. 2011; Nunes et al. 2014; Ribeiro et al. 2015).

The incidence of photolysis and photocatalysis on pharmaceuticals in different water matrices has been investigated as a form of degradation of these CECs. The use of solar light as an activation energy source in heterogeneous photocatalysis has been applied in order to have more sustainable processes. Solar light covers infrared and visible light around 96%, and UV light around 4% (Wetchakun et al. 2019).

In heterogeneous photocatalysis, the light with a certain energy (depending on the semiconductor band-gap) excites the electron from the valence band to the conduction band and creates an electron-hole pair (e^- and h^+). The electrons and holes on the surface of semiconductor participate in reactions that produce reactive oxygen species (ROS) such as hydroxyl radical ($HO^\bullet$), superoxide anion radical ($O_2^{\bullet-}$), singlet oxygen ($^1O_2$), and hydrogen peroxide (H_2O_2) (Zeghioud et al. 2018, 2020; Awfa et al. 2018). The main reactions of each photo-generated active species that promote the catalytic effect are exposed in the reactions shown in Eq. (1)–(8) below:

$$\text{Photocatalyst} + h\nu \rightarrow e_{cb}^- + h^+ \tag{R1}$$

$$h^+ + H_2O \rightarrow HO^\bullet + H^+ \tag{R2}$$

$$h^+ + HO^- \rightarrow HO^\bullet \tag{R3}$$

$$h^+ + \text{Pharmaceutical} \rightarrow \text{Pharmaceutical}^{\bullet+} \rightarrow TPs \tag{R4}$$

$$(O_2)_{\text{ads}} + e_{cb}^- \rightarrow O_2^{\bullet-} \tag{R5}$$

$$O_2^{\bullet-} + H^+ \rightarrow HO_2^\bullet \tag{R6}$$

$$e_{cb}^- + H_2O_2 \rightarrow HO^\bullet + HO^- \tag{R7}$$

$$\text{Pharmaceutical} + ROS \rightarrow TPs \rightarrow CO_2 + H_2O \tag{R8}$$

Currently, several studies of catalysts with better photocatalytic performance are being developed, improving the efficiency under solar irradiation (Tobajas et al. 2017; Khedr et al. 2019; Gómez-Avilés et al. 2019). However, in some cases, the synthesis of the catalyst is expensive which is a disadvantage for the process. In response to this, new perspectives in heterogeneous photocatalysis are focused on the synthesis of economic materials preferably from industrial residues (de O. Pereira et al. 2019). Thus, chemical residues from the galvanic, petrochemical, photographic, and chemical industries have been used as raw material for the synthesis of heterogeneous photocatalysts (da Silva et al. 2014). Nevertheless, the application of photocatalytic treatment methods in the wavelength region of the incident light that leads to the successful use of solar energy has been little studied. Therefore, more studies are required in this area to overcome the limitations of using enough energy for the activation of the reaction in the ultraviolet range (280–390 nm) of the solar spectrum, and the use of this catalyst in real wastewater.

According to previous studies (da Silva et al. 2014), it was reported that the photocatalyst from petrochemical industry has energy band gap (Eg) of 1.78 eV, which means that less radiation energy is required for the activation of the process with a potential use in the visible light region. On the other hand, the high pore volume (1.95 cm^3 g^{-1}), and high surface area (280 m^2 g^{-1}), could promote diffusion of the pharmaceuticals from the solution to the catalyst centers.

In this context, the present study focused on the photodegradation of pharmaceuticals in different aqueous matrices under natural solar radiation. A series of experiments were carried out to explore the use of a solar light-driven photocatalyst from a petrochemical waste and its application in the pharmaceutical degradation in hospital wastewater employing a circumneutral pH. Additionally, these results are complemented by the identification of TPs elucidated through LC-QTOF MS that allowed degradation pathways proposal, and (Q)SAR analysis.

Experimental

Chemicals

All pharmaceuticals (paracetamol-PCT, dipyrone-DIP, and propranolol-PPN) used in this work were analytical grade (purity > 98.99%). For pH adjustment, sulfuric acid (H_2SO_4,

98%) was purchased from Synth (São Paulo, Brazil). Hydrogen peroxide (Synth, 39% w/v) was used as oxidant. All reagents used for chromatographic analyses, LC-MS grade (Lichrosolv®) acetonitrile (ACN) and methanol (MeOH), and formic acid (purity = 98%) were purchased from Merck (Darmstadt, Germany).

Photocatalyst synthesis

Petrochemical waste came from industrial reactors which runs 4th generation Ziegler-Natta catalyst (alfa-olefin polymerizaiton) based on Ti species grafted on Mg- and Si chloro-oxide support. Composition of the waste was Ti/Si = 0.15 and Mg/Si = 0.65. Such slurry was employed for the photocatalyst synthesis.

For the synthesis of the catalyst, modifications were made to the method reported by da Silva et al. (2014).The photocatalyst was synthesized in a mixture ortho-salicylic acid and hydrochloric acid with constant stirring for 12 h. The final waste was calcinated at 450 °C for 4 h. See the schematic description of the experimental setup in Fig. S1 (Supporting information).

Photocatalyst characterization

Parameters as pH, electric potential, conductance, and zeta potential were evaluated in the petrochemical waste (PW) and photocatalyst. The zeta potential (ζ) was analyzed in a Zeta-sizer (Malvern Instruments ZEN3500) with a coherent He-Ne at $\lambda = 632.8$ nm laser as light source. The electrophoretic mobility of each sample was measured three times, and at least 10 runs were performed per measurements and samples were analyzed at 25 °C. The zeta potential was deduced from the electrophoretic mobility (UE) according to Henry's equation and Smoluchoswski approximation (Leite et al. 2018).

Small-angle X-ray scattering (SAXS) measurements were performed at room temperature using the D11A-SAXS line at the Brazilian Synchrotron Light Laboratory (LNLS) (Campinas-SP, Brazil) with wavelength of 1.488 nm. X-ray beam was monochromatized by a silicon monochromator and collimated by a set of slits defining pinhole geometry. Powder samples were placed perpendicular to the X-ray beam, in a sealed 1-mm-thick stainless-steel cell with mica windows. The analysis was performed with X-rays of wavelength equal to $\lambda = 0.1488$ nm, and the detector/channel ratio equal to 0.158. The wave vector range was selected in the range $0.0412 \text{ nm}^{-1} < q < 4.117 \text{ nm}^{-1}$. The average pore radii of the samples were obtained using the Guinier law (Zhi-Hong 2013; Odo et al. 2015). For more information, see text S1.1.

The optical characteristics of the PW and photocatalyst samples were evaluated by diffuse reflectance ultraviolet-visible (DRUV) and diffuse reflectance. A Shimadzu UV-2450 spectrophotometer was used with an ISR-2200

Integrating Sphere Attachment. The baseline in the solid-state was obtained using BaSO$_4$ (Wako Pure Chemical Industries, Ltd.). Kubelka-Munk expression on the diffuse reflectance spectra (DRUV) was applied to determine the band gap from the absorption spectra (Sánchez et al. 2016). For more information, see text S1.2.

The spectra of samples were obtained by infrared spectroscopy in transmittance mode, in the range from 4000 to 400 cm^{-1}, coadding 32 scans, and resolution of 4 cm^{-1}. The samples were measured at room temperature using the equipment Varian 640-IR.

Experimental setup

The synthetic mix-pharmaceutical solution (1000 μg L^{-1} of each pharmaceutical) was prepared freshly every day by appropriate dilution of the pharmaceutical stock solution (1 g L^{-1}) using analytical standards of DIP, PCT, and PPN in distilled water. The choice of these pharmaceuticals was due to the fact that most of them are consumed continuously or in specific cases without medical prescription (e.g., PCT and DIP). Some properties of these pharmaceuticals can be seen in Table S1.

Solar photocatalytic experiments were carried out using a solar batch photo-reactor equipped with an open borosilicate glass beaker (1 L) with full exposure to sunlight and magnetic stirrer. In all experiments, the reaction was started once by adding photocatalyst in appropriate amounts (according to the experimental design) in the mix-pharmaceutical initial solution. Previously, the pH of the initial solution was adjusted using H$_2$SO$_4$ (0.5 mol L^{-1}). Before solar irradiation, the suspensions were allowed to stay in the dark for 15 min under stirring, to reach adsorption equilibrium on the semiconductor surface. At predetermined time intervals, 10 mL aliquot was sampled, centrifuged (5000 revolutions per minute) and then filtered through 0.22-μm PVDF membranes.

These experiments were carried out at the Institute of Chemistry at Universidade Federal do Rio Grande do Sul, RS, Brazil (latitude 30° 4′ 21.0864″ S, longitude 51° 7′ 11.838″ W) using natural sunlight irradiation on a sunny day around noon.

The intensity of sunlight was measured by a solar energy meter (ICEL SP-2000), which provided data in terms of incident radiation (W m^{-2}), the spectral response being in the range 400–700 nm. The sensor was always placed in the position of maximum intensity. Every 2 min, the solar radiation was measured, and the average was calculated for the duration of each experiment. These data were used to calculate the "normalized illumination time" t_{30W} (Miralles-Cuevas et al. 2014), with the proportion of UVA in solar radiation, based on the visible measurement, which facilitates the comparison with other photocatalytic experiments instead of exposition time (t). The intensity of sunlight was almost constant during

the experiments with a mean value of 843 W m^{-2} with an accumulated energy per unit of volume of 33.89 KJ L^{-1}.

Experiments were carried out in three different water matrixes: distilled water (DW), simulated wastewater (SWW), and real hospital wastewater (RHWW). The composition of SWW was adapted from OECD (1999) and simulated the organic content of the raw hospital wastewater. The SWW consisted of peptone 160 mg L^{-1}, beef extract 110 mg L^{-1}, urea 30 mg L^{-1}, Mg$_2$SO$_4$·7H$_2$O 2 mg L^{-1}, and CaCl$_2$·2H$_2$O 4 mg L^{-1}. The RHWW consisted of raw hospital wastewater, which was used as it was collected (without filtration). The main characteristics of this matrix were pH 8.2, chloride 50.7 mg L^{-1}, conductivity 838 μS cm^{-1}, BOD 96 mg L^{-1} O$_2$, TOC 105.4 mg L^{-1}, COD 246 mg L^{-1} O$_2$, phosphate 18.5 mg L^{-1}, total suspended solids 81 mg L^{-1}, and total solids 313 mg L^{-1}.

Experiments in the presence of H$_2$O$_2$ (50 mg L^{-1}) were performed with H$_2$O$_2$ (39% w/v) added to the photo-reactor, which was then exposed to sunlight. Spectral measurements of H$_2$O$_2$ residual were determined by NH$_4$VO$_3$ (Nogueira et al. 2005) method using a Cary 50 UV-Vis spectrophotometer with 1-cm path length cuvette.

Experimental design

Validation spreadsheet (Teófilo and Ferreira 2006) was used to analyze the response of the different independent parameters and calculate the predicted results with the Doehlert experimental design. To investigate the operating conditions for maximum pharmaceuticals degradation performance, pH and photocatalyst dose with different levels were selected. Table 1 elucidates the operating levels and ranges of independent variables evaluated in the present study while Table 2 shows all experimental runs generated using Doehlert design with central point. The pH was in the range of 5–9, and catalyst dose was varied from 50 to 450 mg L^{-1}. The response of the percentage decrease in the summation area of all initial compounds was determined to study the influence of process variables. Four replicates were conducted to calculate the importance of error during the experimental analysis. The analysis

Table 1 Operating levels and ranges of independent variables evaluated

	Parameters			
	Photocatalyst concentration (mg L^{-1})			
Codified value	− 1	− 0.5	0	0.5	1
Experimental value	50	150	250	350	450
	pH			
Codified value	− 0.866		0	0.866
Experimental value	5		7	9

Table 2 Experiments generated using Doehlert design with central point

Experimental design			
Test	Photocatalyst concentration (mg L^{-1})	pH	Decrease area of all initial compounds (%)
1	450	7	9.62
2	350	9	1.52
3	50	7	9.13
4	150	5	0
5	350	5	14.74
6	150	9	6.96
7	250	7	11.01
8	250	7	13.18
9	250	7	10.70
10	250	7	9.20

of variance (ANOVA) was used to analyze the coefficients ($p \leq 0.05$) and the variance explained (%). STATISTICA® software was used to establish the optimal condition through the use of desirability function. All the experiments at this stage were conducted in a random order.

Desirability function is a technique to concurrently determine settings of variables that can give the optimum performance levels for one or more responses. Initially, the response is converted into a particular desirability function that varies from 0 to 1. The desirability 1 is for maximum and desirability 0 is for non-desirable situations or minimum. Therefore, the main advantages of using the desirability function are to obtain qualitative and quantitative responses by the simple and quick transformation of different responses to one measurement (Sakkas et al. 2009).

Analytical methods used for the quantification of pharmaceuticals and identification of their transformation products

Pharmaceuticals degradation and transformation products (TPs) generated during the heterogeneous photocatalysis were monitored by an LC system (Shimadzu Nexera X2) connected to a QTOF mass spectrometer (Bruker Daltonics, Impact II). The LC was equipped with a reverse-phase Hypersil Gold C18 analytical column (2.1 mm × 150 mm × 3 μm). The mobile phase was a mixture of MeOH acidified with 0.1% formic acid (A) and H$_2$O acidified with 0.1% formic acid (B) at a flow rate of 0.5 mL/min. The QTOF-MS instrument was operated with an electrospray ion source ESI in positive mode. Limits of detection (LOD) and quantification (LOQ) for quantification of pharmaceuticals during the treatment processes were calculated based on the signal-to-noise (Table S2,

supporting information). Data from pharmaceuticals and TPs analysis were processed using QuantAnalysis 2.2 software and an automated method supplied by a purpose-built database developed for this application using TargetAnalysis software (Cuervo Lumbaque et al. 2018). In most cases, possible elemental compositions for ions with a deviation of ± 5 ppm were assigned.

In silico (Q)SAR risk assessment

In silico (Q)SAR models were used to predict the toxic risk estimation of the TPs formed throughout photodegradation process. The oral toxicity (Cramer rules) was analyzed using Toxtree (v.3.1.0) by decision tree approach (Patlewicz et al. 2008; Lapenna and Worth 2011). The ecotoxicity assessment of TPs was measured by adopting the Structure-Activity Relationship Model (ECOSAR V2.0). Three aquatic organisms including green algae, Daphnia, and fish were chosen as target objects for biotoxicity exposure assessments. The chronic toxicity values (defined by ChV) of TPs were obtained by means of program calculation. Finally, the biodegradation probability of TPs was predicted through EPI-Suite[TM](US EPA 2019).

Results and discussion

Photocatalysts characterization

The zeta potential distribution graph of photocatalyst is observed in Fig S3 (Supporting information). The PW has a potential value $\zeta = -2.68$ mV at a pH value above 7.44. The values of the photocatalyst at neutral pH are negative ($\zeta = -11.17$ mV), unlike pH 5.0 ($\zeta = +5.64$ mV). On the other hand, samples were kept under agitation for 60 minutes (in the dark), and then the final pH was measured. PW presented significant differences in the final pH (3.0) compared to the initial pH (7.44), and slight changes were evident in the samples that contain the photocatalyst, with pH values of 5.96 and 6.97 for the photocatalyst at initial pH of 5.0 and 7.44 respectively (see Table S3, supporting information). This result can be interpreted considering that the surface of the PW in water has a tendency to preferentially adsorb hydroxyl groups (HO^-) that is, to present behavior of a weak acid, the behavior for the catalyst surface is a weak base. These acid-base characteristics of the surface also determine the adsorption mechanism.

The SAXS analysis of photocatalyst shows two main features, each one present on the Guinier region and the other on the power-law region (Fig. 1(a)). First, the plot (log (I(q)-log(q)) gives us a power-law decay. Furthermore, this power-law decay begins with an exponential regime that appears as inflection reflecting a preferred size. As result, a fractal system composed, with a slope > 4 value. Inset on Fig. 1 (a)
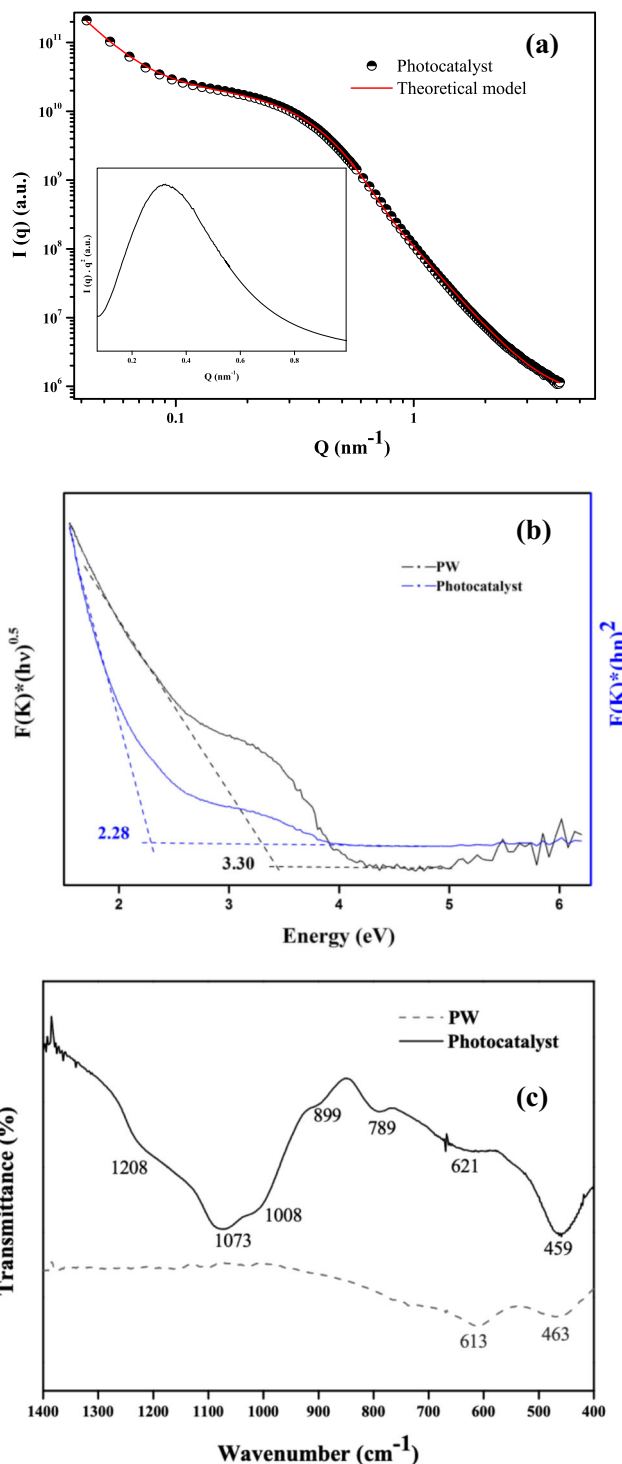
Fig. 1 Characterization photocatalyst. (a) SAXS plot of the photocatalyst sample and Guinier plot. (b) Diffuse reflectance spectra of waste and photocatalyst according to the Kubelka-Munk equation. (c) Infrared spectra of PW and photocatalyst

presents the Kratky plot, ($q^2I(q)$ vs Q). Where was evaluated the cross-sectional radius (R_1) of the particles; as a result, a value of 19 nm. According to Guinier law, the values of 5.2 nm radii of gyration, a pore diameter 14 nm, and a value

of -9.2 of the slope of the Guinier curve were calculated, respectively.

According to the Kubelka-Munk expression, Fig. 1 (b) came from the relations $[F(R)h\nu]^n$ vs $(h\nu)$; $n = 0.5$ (indirect), $n = 2.0$ (direct), presented band gap values of 2.28 eV (indirect) and 3.30 eV (direct) for PW and photocatalyst respectively.

Table S3 shows the vibrational modes of the photocatalyst and PW samples, according to the spectra in the infrared region (Fig. 1(c)). The vibrational modes on the photocatalyst sample on the interval 1400–400 cm^{-1} show bands at 459 cm^{-1} attributed to Ti-O-Ti vibrations on the interconnected octahedral structure, at 621 cm^{-1}, at 789 cm^{-1}, a small shoulder at 899 cm^{-1} related to Ti-O-A, which is very sensitive to the A cation involved on the structure (Ferreira et al. 2006) like Ca(II) specie the value downshift at 880 cm^{-1} or with Co(II) presence an upshift at 916 cm^{-1}. The stretching modes at 1008 cm^{-1} and 1073 cm^{-1} are related to the Si-O bond, and a low intensity band is present at 1208 cm^{-1}. Besides photocatalyst, PW sample **spectrum** has a band at 613 cm^{-1}, and 463 cm^{-1} of the Ti-O-Ti vibration mode.

Doehlert design and desirability function

The optimal condition for pharmaceutical degradation was investigated based on Doehlert design and desirability function. The validation spreadsheet was employed to determine the condition, which increases the removal of pharmaceuticals in DW. According to optimization (Table 2), the optimal conditions for maximum pharmaceutical degradation efficiency (14.74%) in 15 min were 350 mg L^{-1} of photocatalyst at pH 5.0 (test number 5).

The quadratic model explained the experimental values (89.35%); the ANOVA results revealed an excellent agreement between the experimental results and predicted with high significance. Photocatalyst dose was the most significant factor affecting pharmaceutical removal. All results obtained from the Doehlert design, and ANOVA are presented in the supplementary information (section 4S).

The photocatalyst showed negative charge at pH > pH_{PZC} while showed positive charge through at pH < pH_{PZC}. Thus, the solution pH can change the photocatalyst surface that is dispersed in aqueous suspension and showed adsorption/desorption characteristics, which effect the formation of hydroxyl radicals (HO$^{\bullet}$). The results in Table 2 show the basic medium is not favorable for the pharmaceutical removal. The maximum pharmaceutical degradation over basic pH conditions was 6.96%. According to speciation of pharmaceuticals Fig S2 (Supporting information), PCT, DIP, and PPN have a neutral charge at pH 5.0, by increasing the pH values, the negative charge sites in PPN and PCT gradually increases. Hence, this could reduce the degradation of PPN and PCT due of electrostatic repulsion. The positive effect of

photocatalyst at pH 5.0 may reduce the recombination of electrons hole-pair on catalyst surface by taking the electrons from the conduction band.

The optimization procedure was performed through the desirability function approach (Fig. 2). On the left side of Fig. 2 (below), the individual desirability scores for the photocatalytic efficiency of pharmaceutical degradation are illustrated, with desirability being 1.0 as the object value; the current level of each factor in the model is represented in the upper (left) part of Fig. 2. These figures allow seeing the changes in the level of each variable and the direct incidence of the response (% area decrease) and the general desirability, Fig. 2 indicated that a decrease in pH values and an increase of catalyst dose resulted in increased pharmaceutical removal. On the basis of these estimates and choosing desirability score of 1, software optimized 17.93% degradation of pharmaceutical with calculating the optimized model variables of photocatalyst 450 mg L^{-1} at pH 5.0. Otherwise, 350 mg L^{-1} dose of catalyst is within the range of acceptable values according to the desirability function and this value does not represent significant differences compared to the individual desirability score of the maximum dose of catalyst. Therefore, decreasing the amounts of catalyst used in the reaction reduces the cost of the process. For this reason, 350 mg L^{-1} and pH 5 were the selected conditions for the following stages of experiments in DW, SWW, and RHWW matrices.

Solar photocatalytic treatments

Preliminary experiments were conducted to assess the extent of substrate (i) adsorption onto the catalyst surface, in the dark (Fig. 3(a)), and (ii) photodegradation in the absence of catalyst for a t_{30W} of 161.8 min (Fig. 3(b)).When corresponding experiment was done in the dark, the efficiency in the adsorption was negligible. This is demonstrated in Fig. 3(a), which indicates only slight adsorption by PPN (10.3%), PCT (6.4%), and DIP (2.4%) in 180 min. Given that the point of zero charge of catalysts is 5.7, at 5.0 > pH > 5.7, there is not electrostatic attraction between the positive charged catalyst surface and pharmaceuticals. On the other hand, pharmaceutical removal by direct photodegradation is depicted in Fig. 3 (b). As shown, direct photolysis seemed to be mostly effective for DIP than PCT and PPN, a DIP removal close to 46% in t_{30W} of 58.7 min and after 100 min of t_{30W}, DIP and PPN were degraded in 87.5% and 23.2%, respectively. The fast degradation of DIP can be deduced by the photoexcitation of pyrazole at the longest wavelengths to involve $\pi^* \rightarrow \pi$ excitation, besides, photolysis at UVC radiation is characterized by N–H bond fission (King et al. 2010). Gómez et al. (2008) also confirmed the easy degradation of DIP under direct photolysis using a solar UV Solar simulator. PPN shows greater degradation after t_{30W} 113 min, at this time, the total accumulated energy at the reactor turned out to be 33.89 kJ L^{-1}, which
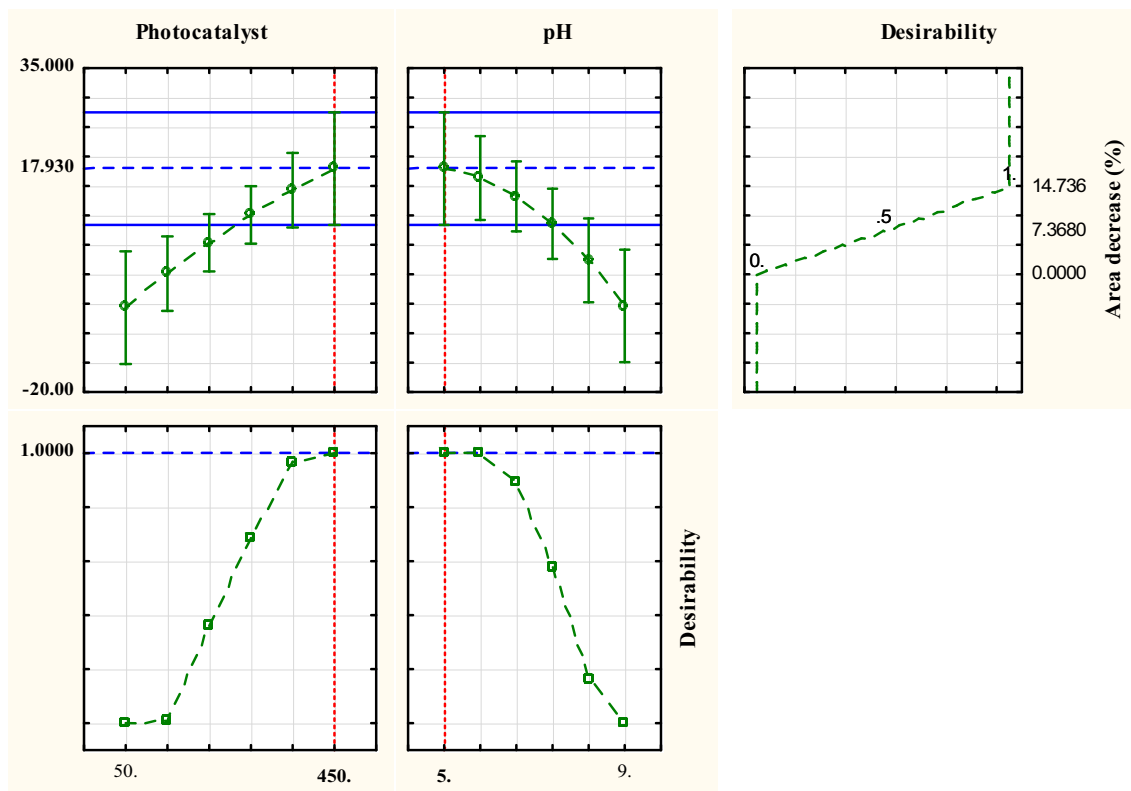
Fig. 2 Profiles for predicated values and desirability function for pharmaceutical degradation (%). Dashed line indicated current values after optimization

means that much more accumulated energy is needed to achieve direct photodegradation of PPN. According to Dantas et al. (2010), PPN undergoes photolysis in its protonated state by the amino group, which in this structure is the priority reaction center. In contrast, PCT photolysis is negligible. According to Yang et al. (2008), degradation of PCT is more efficient with UVC radiation (254 nm) than UVA radiation (365 nm), and solar ultraviolet global irradiance (290–385 nm) (Foyo-Moreno et al. 1999) only covers a small part of UV radiation; consequently, a negligible amount of this pharmaceutical product is degraded.

Effect of catalyst on pharmaceutical photo-oxidation removal is shown in Fig. 3(c), and degradation of DIP and PPN suggested that the photodegradation was related to ROS influenced by catalyst; after an irradiation time higher than t_{30W} of 58.7 min, the DIP complete removal was achieved (less than the LOD of the method, $< 0.36\ \mu g\ L^{-1}$) and after of t_{30W} of 161.8 min, PPN degradation was accomplished (less than the LOD of the method, $< 0.03\ \mu g\ L^{-1}$). This result confirms the positive effect of catalyst on pharmaceutical photo-removal. The photolytic and photocatalytic degradation can be achieved by direct reaction with photons produced by UV, and/or by indirect reaction with ROS radicals produced by the reaction between H_2O and catalyst. However, ROS generation in photocatalysis of pharmaceutical products is greater than photolysis.

The solution pH influences the ionization states of catalyst and the pharmaceuticals. This explains, in part, the results of Fig. 3 (c) where some effects involving (i) the equilibrium of water dissociation which, in turn, affects the level of radicals generation, and (ii) the oxidative power of the photogenerated holes (Ioannou et al. 2011). According to radicals generation, the pH has an influence on the performance of ROS and other subsequent reactions. The hydroxyl radical is generated from reactions between adsorbed water and h^+ generated by catalyst activation, being the preferred radical species for the degradation of pharmaceuticals due to its high redox standard potential $E°'(HO^•/H_2O) = 2.34$ V (Collin 2019). Notwithstanding this, when the valence band (E_{VB}) of the photocatalyst is insufficient to catalyze the production of $HO^•$, superoxide radicals could be a dominant species ($O_2 + e^- \rightarrow O_2^{•-}$) (Teoh et al. 2012), despite the fact that these species are a weaker oxidant source ($E°'(O_2^{•-}/H_2O_2) = 0.93$ V) in comparison with $HO^•$. Likewise, other reactive oxygen species such as singlet oxygen ($^1O_2$), which represents an excited state of O_2, can also participate in the reactions (Diaz-Angulo et al. 2019).

The pKa values for the hydroperoxyl radical ($HO_2^•/O_2^{•-}$) and hydroxyl radical ($HO^•/O^{•-}$) are 4.8 and 11.9, respectively (Collin 2019). Therefore, relative to pH in degradation experiments (around 5.0), it is probable that $O_2^{•-}$ and $HO^•$ are the most predominant species in the reaction. Some studies also
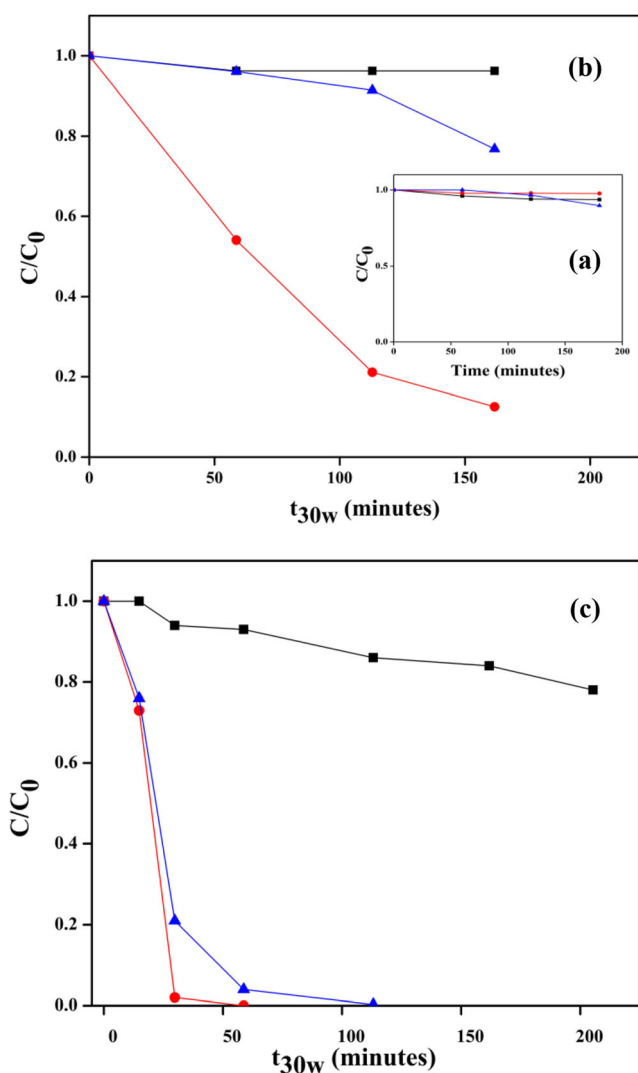
Fig. 3 Removal of pharmaceuticals in DW matrix. (a) adsoption (dark). (b) photolysis (solar). (c) solar photo-catalysis. Conditions: 350 mg L^{-1} at pH 5.0 (——▲——) PPN, (——●——) DIP, (——■——) PCT

reported the high contribution of the hole (h^+), and $O_2^{\bullet-}$ in photocatalytic degradation of the mono-, bi-, and tri-compound systems at circumneutral pH (Zeghioud et al. 2019).

The structural characteristics of compounds, such as ring substitutions and the nature of the aliphatic chain, have an impact on the susceptibility to degradation (Fathinia et al. 2015). At the same time, HO$^\bullet$ has a strong electrophilic feature, which preferentially attacks groups or carbon atom of the aromatic ring with high electron density (Marusawa et al. 2002; Fathinia et al. 2015). In DIP, HO$^\bullet$ or $O_2^{\bullet-}$ attack occurs mostly at the position of the pyrazole ring activated by the presence of substituents. The pyrazole ring of DIP is resistant to oxidation and reduction but the alkyl groups attached to the ring can be oxidized by ROS to the respective acids. The presence of both electronegative nitrogen atoms in the pyrazole ring reduces the electron density of the C_3 and C_5

positions leaving electron density of C_4 position unaltered; thus, the C_4 position is vulnerable to electrophilic attack (Ji Ram et al. 2019). This fact can be seen in more detail in transformation product section.

In PPN, the presence of hydroxyl and alkoxy groups (electron-donating groups) in its molecular structure can intensify the resonance effect and consequently, increase the removal efficiency of PPN. On the other hand, PCT is mainly oxidized via hydroxylation by HO$^\bullet$. For example, Yang et al. (2009) described that HO$^\bullet$ is the only oxidant that can promote PCT degradation since the molecule does not contain a strong electron donating group to allow degradation pathways such as electron transfer. However, as mentioned above, heterogeneous photocatalysis involves the participation of other oxidizing species other than HO$^\bullet$, such as $O_2^{\bullet-}$ and $^1O_2$. The low percentage of PCT degradation (< 20%) is in agreement with other studies (Díez-Mato et al. 2014; Diaz-Angulo et al. 2019), where elimination of PCT was rather limited by $^1O_2$ as predominant oxidant specie in heterogeneous photocatalysis.

Matrix effect

The effectiveness of the photocatalysts in a more realistic application was studied using a SWW and RHWW matrices spiked with DIP, PCT, and PPN. Photo-degradation runs are show in the Fig. 4 (a, b). For DIP, > 99% (less than the LOD of the method) and 99% removal were achieved for the SWW and RHWW after t_{30w} 58.7 and 205.4 min, respectively, while relatively lower removal of PPN (about 90% and 71%) was observed in SWW and RHWW. This is owing to matrix effect, i.e., the presence of a larger number of organic molecules compared to DW matrix compete to react with the same concentration of HO$^\bullet$ or are absorbed into the catalyst blocking the flow of electrons, since organic matter (OM) is known to be extremely stable under photocatalytic and other advanced oxidation conditions (Dialynas et al. 2008). ROS are partly consumed to attack OM and this explains the reduced performance in SWW and RHWW in comparison with DW. Furthermore, the presence of chlorides (50.7 mg L^{-1}) could act as radical scavengers (Ioannou et al. 2011), as well as the other ions in RHWW could participate in the modification of the surface electrical charge by ionic force (Lado Ribeiro et al. 2019).

The percentage of PCT degradation in SWW was 56%. This higher value compared to the results obtained in DW (22%) can be explained by ROS generated by often chromophoric natural organic matter (NOM) under solar irradiation. The urea monomers in SWW matrix, which can incorporate water in an extensive hydrogen-bonding network, result in the release chromophoric natural organic matter (NOM) that can be excited by light, which increased singlet oxygen levels (Riyajan et al. 2003). NOM absorbs sunlight to form a
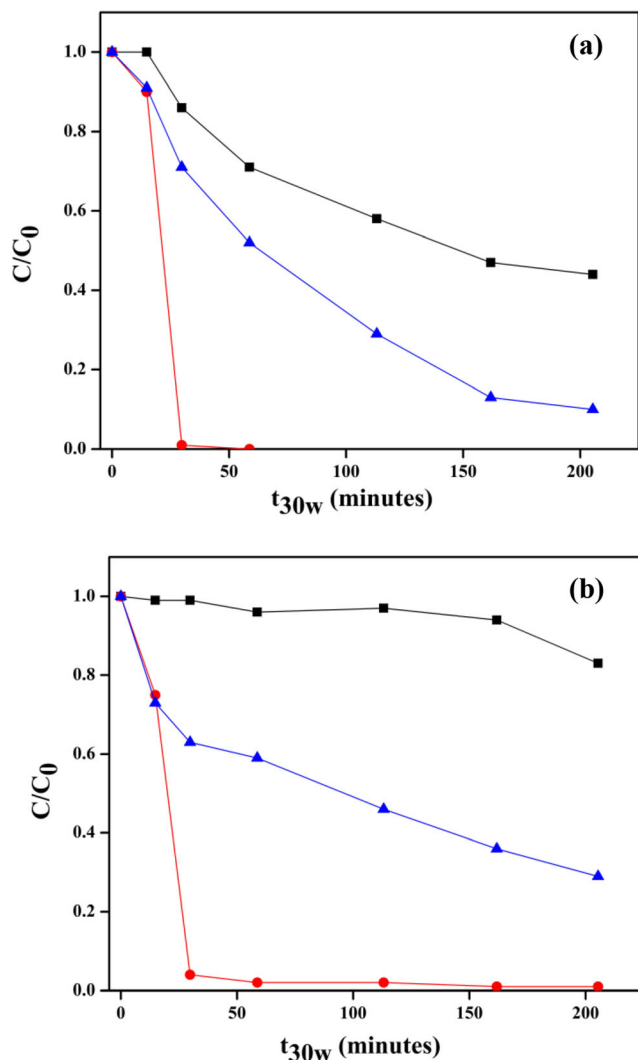
Fig. 4 Matrix effect. (a) SWW matrix. (b) RHWW matrix. Conditions: 350 mg L^{-1} at pH 5.0 (———▲———) PPN, (———●———) DIP, (———■———) PCT

singlet-excited state (^{1}NOM*), directly a small fraction of this transfers to a triplet excited state (^{3}NOM*) through intersystem crossing (ISC), and consecutively ^{3}NOM* reacts with dissolved oxygen to produce singlet oxygen ($^1O_2$), following with energy and intramolecular electron transfer for photochemical formation of HO$^•$ and $O_2^{•-}$ from NOM (Xu et al. 2011; Li et al. 2017).

In addition, according to the characterization of the photocatalyst, Ti-O-A involves cation on the structure such as Ca(II) and Co(II), which could react with the urea present in the SWW. Urea could be a precursor of photocatalysts, due to the strong interaction between metals and the solitary pair of oxygen electrons present in this molecule; thus, metals can capture an oxygen atom from urea promoting the generation of ROS, providing a better response in the visible-light (Cheng et al. 2008) and reduced charge recombination (Yan et al. 2019).

Hence, PCT degradation in SWW is induced by oxidation with ROS generated by urea. In addition to this, studies carried out by Li et al. (2017) and Sikorski (2014) suggested that NOM reacts with phenolic compounds to yield phenoxyl radical to the involvement of photoproduced ROS. The difference in PCT decomposition rates in SWW (56 %) and RHWW (17%) could be due to the inhibitory effects of the coexisting substances in RHWW explained above and the absence of NOM.

On the other hand, according to the behavior of pharmaceuticals degradation, DIP degradation in all matrices and PPN in DW showed faster initial decomposition rates and higher degradation capacity in the first minutes of treatment, after which the efficiencies diminished. This behavior could be explained using the method described by Chan and Chu (2003), resulting in coefficients of determination (R^2) in the range from 0.95 to 1.00. PCT degradation in SWW could be explained by pseudo-second-order kinetics ($R^2 = 0.98$). In turn, the degradation behavior of PPN in SWW presented pseudo-first-order kinetics ($R^2 = 0.99$) and the PPN data in RHWW fit to pseudo-second order ($R^2 = 0.97$).

Effect of hydrogen peroxide addition

The effect of combining natural sunlight, photocatalyst, and H_2O_2 (50 mg L^{-1}) as oxidant on pharmaceutical removal in RHWW was subsequently studied. As seen in Fig. 5, the use of additional oxidant had a slightly beneficial effect on the degradation of PPN, while it did not clearly improve the degradation of DIP and PCT compared to the respective runs without H_2O_2. PPN degradation followed a pseudo-first-order kinetic ($R^2 = 0.99$), and the degradation efficiency of PPN is reflected in k values from 0.011 min^{-1} (SWW) to 0.018 min^{-1} (RHWW with H_2O_2).
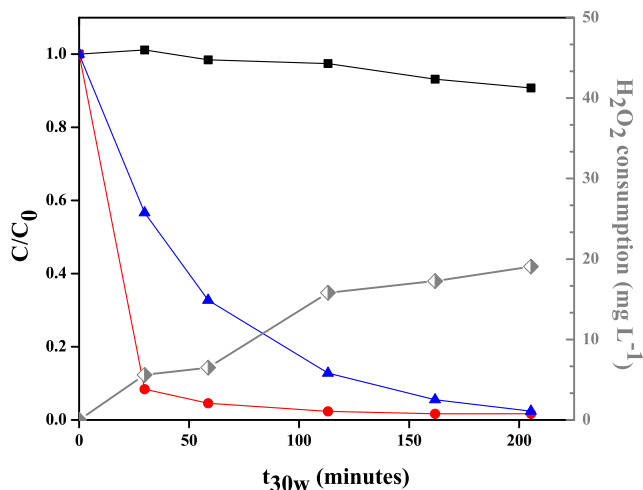
Fig. 5 Degradation of pharmaceuticals with addition of H_2O_2. Conditions: 350 mg L^{-1} at pH 5.0 (———▲———) PPN, (———●———) DIP, (———■———) PCT, (———◇———) H_2O_2

However, H_2O_2 consumption was around 20 mg L^{-1} (Fig. 5) throughout the process, which suggested that H_2O_2 was not effectively coupled with a photocatalyst. This could be explained by the action of the organic matter present in RHWW that is adsorbed on the surface of the catalyst, decreasing the synergy between the components of the photocatalysis. This finding is rather unexpected since H_2O_2 usually has a beneficial role reacting. Consequently, the addition of oxidant does not affect the electron-hole recombination of the photocatalyst, which is reflected in a low acceptance of electrons in the conduction band; therefore, the amount of generation of $HO^{\bullet}$ and other oxidizing species is not efficient. Another possible effect of the restriction of pharmaceutical degradation with H_2O_2 is the presence of dissolved oxygen, since this acts as an efficient electron scavenger producing the superoxide radical anion ($E°'(O_2/O_2^{\bullet-}) = -0.33$ V), which does not significantly improve the degradation taking into account the low oxidation potential of this species ($E°'(O_2^{\bullet-}/H_2O_2) = 0.93$ V) (Collin 2019).

Transformation products identification

In this case, up to 20 different TPs could be identified, which are depicted in Fig. 6. Table S5 shows the measured and calculated exact masses of the protonated ions, the error between them, and the proposed empirical formula

corresponding to the compounds identified by LC-QTOF MS. The proposals for the degradation pathways were made based on the formation of hydroxyl radicals in the system; however, these same TPs may have arisen from the reaction with other ROS mentioned in previous sections.

DIP is rapidly hydrolysed to 4-methylaminoantipyrine (4-MAA)-.This reaction is proton-dependent, facilitated in an aqueous medium, and enhanced by the thermodynamic stability of the product (Bacil et al. 2018). 4-MAA oxidation occurs in the enamine moiety following three different reaction pathways: (i) opening of the pyrazolone ring (route I); (ii) hydroxylation on the pyrazolone ring (route II); and (iii) formation and oxidation of metabolites, mainly in the RHWW matrix (route III) Fig. 6 (a).

In route I, the pyrazolinone moiety was continuously hydroxylated and oxidized to TP32 DIP found in the SWW matrix. On the other hand, the pyrazolone ring opening was assessed by the identification of TP7 DIP (1-acetyl-1-methyl-2-aminomethyl-oxa-moyl-2-phenylhydrazide), which lead to the loss of oxamoyl chain to yield TP10 DIP. On the other hand, the loss of methyl presents in 4-MAA and its continuous oxidation generates TP9 DIP (route II). The identification of TP5 DIP shows a new proposal for the opening of the pyrazolone ring. The structure suggests cleavage of the N-N bond to provide a multiple hydroxylated derivative. This formula corresponded to the addition of two oxygen atoms to the
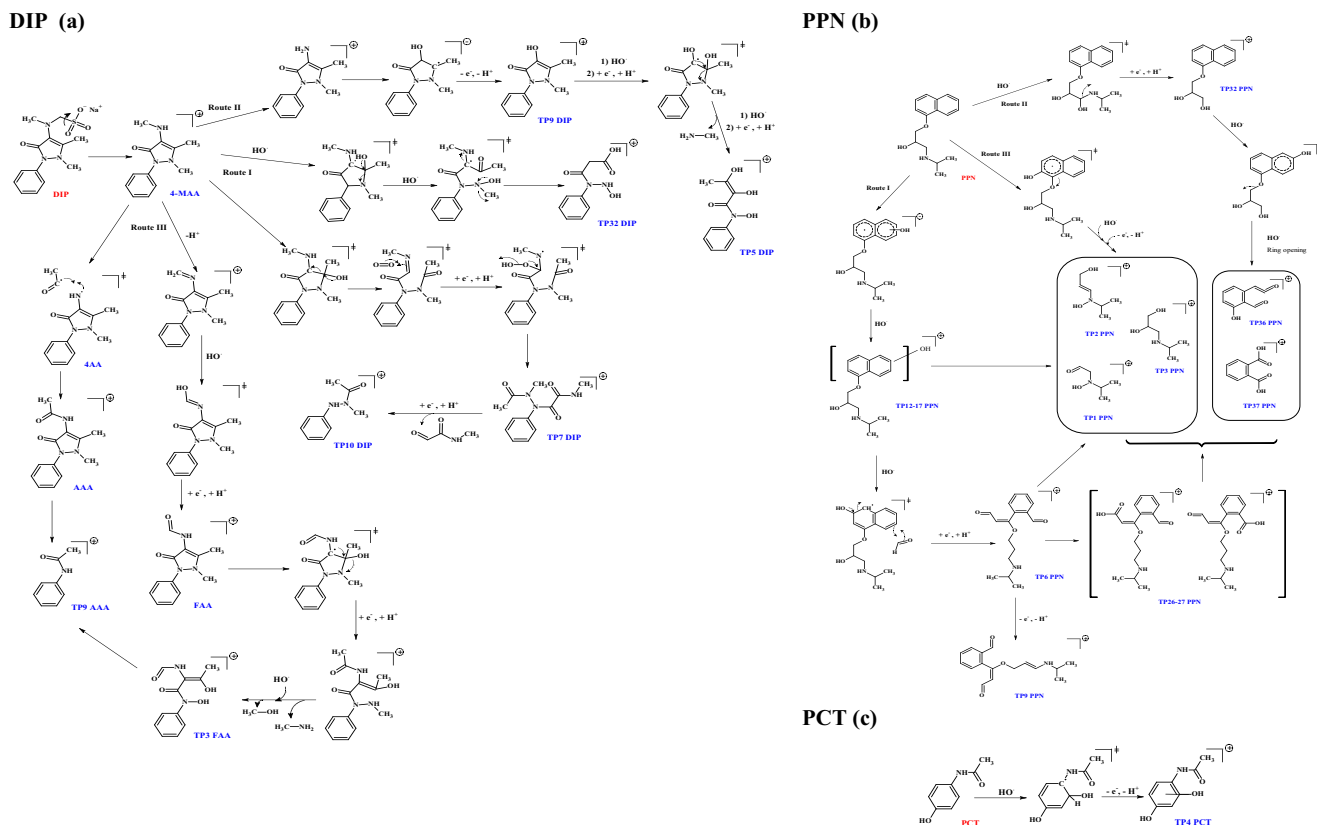

Fig. 6 Transformation products (TPs) identified by LC-QTOF MS in heterogeneous sunlight-driven photocatalysis. (a) DIP; (b) PPN; (c) PCT

TP9 DIP structure and to the loss of the amino moiety. TP5, TP7, TP9, and TP10 DIP has been reported as TPs of DIP in photodegradation study performed by Gómez et al. (2008).

Route III focuses on DIP metabolites and their oxidation, 4-MAA via demethylation yield to 4-aminoantipyrine (4AA). This reaction is irreversible and pH dependent (Bacil et al. 2018). The 4AA further acetylated to acetylaminoantipyrine (AAA); 4-formylaminoantipyrine (FAA) is generated by oxidation of the n-methyl group from 4-MAA. The subsequent opening of the pyrazolone ring and constant oxidation produces TP3 FAA. Finally, TP9 AAA could be produced from AAA and TP3 FAA.

A plausible reaction sequence for the oxidation of PPN by ROS was proposed based on the identified TPs. Three reaction pathways were proposed as seen in Fig. 6 (b). The first path is (i) hydroxylation and opening of the naphthol ring; (ii) attack at the secondary amine group; and (iii) ether cleavage products. In the first path, the constitutional isomers TP12 PPN and TP17PPN ($C_{16}H_{22}NO_3$, m/z 276.1584), which represent the addition of hydroxyl radical to the parent compound, yield to monohydroxylated intermediates. TP6 PPN is a naphthol ring-opening product from $C_{16}H_{22}NO_3$, m/z 276.1584. TP6 PPN is commonly detected in solar experiments (Santiago-Morales et al. 2013). Consecutive hydroxylation of TP6 PPN can generate a compound with m/z 308.1495 and $C_{16}H_{22}NO_5$, with a carboxylic acid in its structure. This TP can be represented through two structures (TP26 PPN or TP27 PPN), and no characteristic fragment was observed in MS, not allowing unambiguous identification in this situation. TP9 PPN may originate from TP6 PPN; the structure suggests double bond formation in the aliphatic chain.

The second pathway started by ROS attack at the secondary amine group, leading to the formation of di-hydroxyl propoxyl naphthalene (TP32 PPN) (Ganiyu et al. 2017). The oxidative cleavage of α-naftol moiety with HO• yield TP36 PPN and TP37 PPN (phthalic acid) (Ganiyu et al. 2017); these last both TPs can also be TPs of the other aromatic compounds identified in the degradation pathways of PPN. The oxidative cleavage of the aliphatic intermediates leads to the formation of alcohol (TP2 PPN and TP3 PPN) and short-chain aldehyde (TP1 PPN). TP2 PPN and TP3 PPN are attributed to the direct cleavage of the ether bond of PNN and subsequent oxidation (path III) or it can be caused by the rupture of the ether bond in the TPs mentioned above. In turn, TP1 PPN could also be attributed to the direct cleavage of the aliphatic chain of the PPN molecule or the different TPs to obtain the corresponding aldehyde. The TPs presented in the first and third path were also identified by Santiago-Morales et al. (2013) in photocatalytic degradation of PPN using Ce-doped TiO$_2$.

Otherwise, the TP4 PCT (Fig. 6(c)) involves attack of HO• radical onto the aromatic ring of PCT to give ortho-, meta-, or para-hydroxylation (Moctezuma et al. 2012).

The relative occurrence-formation of the main identified TPs is given in Fig. S5 (Supporting information). The most plentiful TPs obtained in photocatalytic tests were TP9 AAA, TP7 DIP, TP10 DIP, and AAA, which are attributed to the oxidation of DIP in pathways III and I. In contrast, TP1 PPN, TP2 PPN, TP32 PPN, and TP36 PPN were measured in relatively high intensity compared to the other TPs of PPN. This indicates a higher amount of aliphatic and aromatic chain of low carbon number; these compounds, therefore, are more sensitive to biological degradation than other TPs. TP4 PCT has a low occurrence-formation compared to the other TPs, after t_{30W} of 30 min the area of this TP showed a decrease until the final time of monitoring.

In general, degradation of pharmaceuticals through solar light-driven photocatalyst from petrochemical waste increased the accumulation of hydroxy and polyhydroxy intermediates, with less formation of aliphatic products, which favors the increase of polyhydroxylated intermediates in the matrices. This could be attributed to the low oxidizing power of the photocatalytic system, which increases the accumulation of the first oxidation TPs. Most of the TPs tended to accumulate throughout the solar process, exhibiting a significant increase in t_{30W} of 30 min and a continual presence throughout the monitored treatment time.

(Q)SAR analysis: TPs toxicity and biodegradability assessment by using in silico predictions

(Q)SAR analysis was applied to predict chronic toxicity values (ChVs) by ECOSAR program for previously identified TPs (see Table S6, Supporting information).

The ChVs of pharmaceuticals and their TPs were associated according to the Chinese hazard evaluation guidelines for new chemical substances (HJ/T 154-2004). 4-MAA is classified as chronically not harmful (ChV > 10 mg L^{-1}) at all three trophic levels. The ChVs for PPN were predicted to be 0.951 mg L^{-1} for fish, 0.227 mg L^{-1} for Daphnia, and 0.657 mg L^{-1} for green algae. According to these values, PPN was classified chronically toxic (0.1 < ChV < 1.0 mg L^{-1}) at all three trophic levels. The values of PCT for fish (26.5 mg L^{-1}) and green algae (37 mg L^{-1}) are classified as chronically not harmful (ChV > 10 mg L^{-1}) while Daphnia (5.12 mg L^{-1}) is considered harmful (1.0 < ChV < 10 mg L^{-1}). As shown in Table S6 (Supporting information), the DIP's TPs were generally more toxic to green algae compared to the other organisms. This is explained due to the presence of the hydrazine group in the structures of the DIP's TPs, this group is highly toxic to green algae (CERI 2007).

To better understand the toxicity impact of TPs formed during the photocatalytic degradation of pharmaceuticals, the ChV of pharmaceuticals were used to normalize TPs (ChV) data. Figure S6 shows the normalization of more toxic TPs (ChV < 1 mg L^{-1}); values less than 1 represent a greater

toxicity impact compared to the pharmaceutical. According to Fig. S6 and Table S6, most DIP´s TPs represent more toxicity than the 4-MAA; TP9 DIP, TP 10 DIP, AAA, and FAA are 100 times more toxic (Green algae) than 4-MAA. These TPs at the three trophic levels showed an increase in toxicity between 10 and 100 times greater than the starting compound and according to relative abundance; also, these TPs are abundant in DIP degradation. On the other hand, the TPs of PPN showed that the oxidation process can decrease the toxicity of target pharmaceutical since, according to normalization, the identified compounds values are greater than 1 Table S6 (Supporting information). Finally, TP4 PCT indicated more relevant toxicity in fish and green algae than PCT.

Most of the TPs identified were persistent (75%) with low biodegradation capacity, with 35% of the TPs above the threshold of toxicological concern (TTC, Cramer class III classification). This could suggest significant toxicity with a significant risk to human health. Therefore, it is necessary to further assess the environmental risk of oxidation of pharmaceuticals in aquatic environment matrices in future studies.

Conclusions

The petrochemical waste-based photocatalyst was studied as a suitable material for pharmaceutical degradation in different matrices at a pH close to neutral. According to the results of the characterization, significant differences have been observed between the PW and the photocatalyst such as vibrational modes, optical absorption gap, and acid-basic characteristics on the surface, which suggests the potential use of the photocatalyst in the water and wastewater treatment. The efficient degradation was DIP> PPN > PCT, being DIP highly sensitive to photolysis. Experiments carried out in RHWW spiked with pharmaceuticals showed a low rate for the photocatalytic process compared with DW and SWW mainly to DIP and PPN. This could be attributed to the presence of radical scavengers but also to substances competing for surface adsorption. Twenty TPs were detected by means of exact mass measurements performed by LC-QTOF MS. The main TPs derived from the addition of hydroxyl groups to the aromatic nuclei or to the ring-opening attack. The (Q)SAR analysis showed the formation of toxic TPs mostly from DIP, which accumulated in time of experiment photocatalytic. Therefore, it is necessary for further assessment of environmental risk of TPs in ambient aquatic environments in future studies.

Authors' contributions *Elisabeth Cuervo Lumbaque*: Investigation, Formal analysis, Writing - Original Draft, Visualization

Cálita Elis Schweigert: Investigation, Formal analysis

Leonardo Oliveira dos Santos: Investigation, Formal analysis

Vladimir Lavayen: Investigation; Formal analysis, Writing - Original Draft

João Henrique Z. dos Santos: Conceptualization, Writing - Original Draft

Carla Sirtori: Conceptualization, Writing - Original Draft, Supervision, Project administration, Funding acquisition

Data availability Additional results and materials are available by contacting the authors via email.

Compliance with ethical standards

Ethical approval This study was approved by the Ethics Committee (CAAE: 66594317800005327, project: 2017-0170).

Consent to participate Not applicable to this study.
Consent to publish

All authors and funding agencies authorize the publication of this study.
Competing interests The authors declare that they have no competing interests.

References

Awfa D, Ateia M, Fujii M, Johnson MS, Yoshimura C (2018) Photodegradation of pharmaceuticals and personal care products in water treatment using carbonaceous-TiO$_2$ composites: a critical review of recent literature. Water Res 142:26–45. https://doi.org/10.1016/J.WATRES.2018.05.036

Bacil RP, Buoro RM, Campos OS, Ramos MA, Sanz CG, Serrano SHP (2018) Electrochemical behaviour of dipyrone (metamizole) and others pyrazolones. Electrochim Acta 273:358–366. https://doi.org/10.1016/j.electacta.2018.04.082

Becker RW, Ibáñez M, Lumbaque EC et al (2020) Investigation of pharmaceuticals and their metabolites in Brazilian hospital wastewater by LC-QTOF MS screening combined with a preliminary exposure and in silico risk assessment. Sci Total Environ 699:134218. https://doi.org/10.1016/J.SCITOTENV.2019.134218

Čelić M, Gros M, Farré M, Barceló D, Petrović M (2019) Pharmaceuticals as chemical markers of wastewater contamination in the vulnerable area of the Ebro Delta (Spain). Sci Total Environ 652:952–963. https://doi.org/10.1016/J.SCITOTENV.2018.10.290

Chan KH, Chu W (2003) Modeling the reaction kinetics of Fenton's process on the removal of atrazine. Chemosphere 51:305–311. https://doi.org/10.1016/S0045-6535(02)00812-3

Chemicals Evaluation and Research Institute (CERI) (2007) Hazard assessment report-Hydrazine CAS No. 302-01-2. Japan

Cheng P, Deng C, Gu M, Dai X (2008) Effect of urea on the photoactivity of titania powder prepared by sol–gel method. Mater Chem Phys 107:77–81

Chung S, Brooks BW (2019) Identifying household pharmaceutical waste characteristics and population behaviors in one of the most densely populated global cities. Resour Conserv Recycl 140:267–277. https://doi.org/10.1016/J.RESCONREC.2018.09.024

Collin F (2019) Chemical basis of reactive oxygen species reactivity and involvement in neurodegenerative diseases. Int J Mol Sci 20:2407

Cuervo Lumbaque E, Cardoso RM, Dallegrave A, dos Santos LO, Ibáñez M, Hernández F, Sirtori C (2018) Pharmaceutical removal from different water matrixes by Fenton process at near-neutral pH: Doehlert design and transformation products identification by UHPLC-QTOF MS using a purpose-built database. J Environ Chem Eng 6:3951–3961. https://doi.org/10.1016/J.JECE.2018.05.051

da Silva WL, Lansarin MA, Stedile FC, dos Santos JHZ (2014) The potential of chemical industrial and academic wastes as a source of supported photocatalysts. J Mol Catal A Chem 393:125–133. https://doi.org/10.1016/J.MOLCATA.2014.05.040

Dantas RF, Rossiter O, Teixeira AKR, Simões ASM, da Silva VL (2010) Direct UV photolysis of propranolol and metronidazole in aqueous solution. Chem Eng J 158:143–147

de O. Pereira L, de Moura SG, Coelho GCM et al (2019) Magnetic photocatalysts from industrial residues and TiO₂ for the degradation of organic contaminants. J Environ Chem Eng 7:102826. https://doi.org/10.1016/J.JECE.2018.102826

Dialynas E, Mantzavinos D, Diamadopoulos E (2008) Advanced treatment of the reverse osmosis concentrate produced during reclamation of municipal wastewater. Water Res 42(18):4603–4608

Diaz-Angulo J, Porras J, Mueses M, Torres-Palma RA, Hernandez-Ramirez A, Machuca-Martinez F (2019) Coupling of heterogeneous photocatalysis and photosensitized oxidation for diclofenac degradation: role of the oxidant species. J Photochem Photobiol A Chem 383:112015

Díez-Mato E, Cortezón-Tamarit FC, Bogialli S, García-Fresnadillo D, Marazuela MD (2014) Phototransformation of model micropollutants in water samples by photocatalytic singlet oxygen production in heterogeneous medium. Appl Catal B Environ 160–161:445–455. https://doi.org/10.1016/j.apcatb.2014.05.050

Fathinia M, Khataee A, Naseri A, Aber S (2015) Monitoring simultaneous photocatalytic-ozonation of mixture of pharmaceuticals in the presence of immobilized TiO₂ nanoparticles using MCR-ALS: identification of intermediates and multi-response optimization approach. Spectrochim Acta Part A Mol Biomol Spectrosc 136:1275–1290. https://doi.org/10.1016/j.saa.2014.10.014

Ferreira OP, Souza Filho AG, Mendes Filho J, Alves OL (2006) Unveiling the structure and composition of titanium oxide nanotubes through ion exchange chemical reactions and thermal decomposition processes. J Braz Chem Soc 17:393–402

Foyo-Moreno I, Vida J, Alados-Arboledas L (1999) A simple all weather model to estimate ultraviolet solar radiation (290–385 nm). J Appl Meteorol 38:1020–1026

Ganiyu SO, Oturan N, Raffy S, Esposito G, van Hullebusch ED, Cretin M, Oturan MA (2017) Use of sub-stoichiometric titanium oxide as a ceramic electrode in anodic oxidation and electro-fenton degradation of the beta-blocker propranolol: degradation kinetics and mineralization pathway. Electrochim Acta 242:344–354. https://doi.org/10.1016/J.ELECTACTA.2017.05.047

Gómez MJ, Sirtori C, Mezcua M et al (2008) Photodegradation study of three dipyrone metabolites in various water systems: Identification and toxicity of their photodegradation products. Water Res 42:2698–2706. https://doi.org/10.1016/j.watres.2008.01.022

Gómez-Avilés A, Peñas-Garzón M, Bedia J, Rodriguez JJ, Belver C (2019) C-modified TiO₂ using lignin as carbon precursor for the solar photocatalytic degradation of acetaminophen. Chem Eng J 358:1574–1582. https://doi.org/10.1016/J.CEJ.2018.10.154

Ioannou LA, Hapeshi E, Vasquez MI, Mantzavinos D, Fatta-Kassinos D (2011) Solar/TiO₂ photocatalytic decomposition of β-blockers atenolol and propranolol in water and wastewater. Sol Energy 85:1915–1926. https://doi.org/10.1016/j.solener.2011.04.031

Ji Ram V, Sethi A, Nath M, Pratap R (2019) Chapter 5 - Five-Membered Heterocycles. The Chemistry of Heterocycles, 1st edn. Elsevier, pp 149–478

Khedr TM, El-Sheikh SM, Ismail AA, Bahnemann DW (2019) Highly efficient solar light-assisted TiO₂ nanocrystalline for photodegradation of ibuprofen drug. Opt Mater (Amst) 88:117–127. https://doi.org/10.1016/J.OPTMAT.2018.11.027

King GA, Oliver TAA, Nix MGD, Ashfold MNR (2010) Exploring the mechanisms of H atom loss in simple azoles: ultraviolet photolysis of pyrazole and triazole. J Chem Phy 132:02B604

Lado Ribeiro AR, Moreira NFF, Li Puma G, Silva AMT (2019) Impact of water matrix on the removal of micropollutants by advanced oxidation technologies. Chem Eng J 363:155–173. https://doi.org/10.1016/J.CEJ.2019.01.080

Lapenna S, Worth A (2011) Analysis of the Cramer classification scheme for oral systemic toxicity-implications for its implementation in Toxtree. JRC Sci Tech Rep EUR 24898:1–27

Leite DC, Kakorin S, Hertle Y, Hellweg T, da Silveira NP (2018) Smart starch–poly (N-isopropylacrylamide) hybrid microgels: synthesis, structure, and swelling behavior. Langmuir 34:10943–10954

Li Y, Pan Y, Lian L, Yan S, Song W, Yang X (2017) Photosensitized degradation of acetaminophen in natural organic matter solutions: the role of triplet states and oxygen. Water Res 109:266–273. https://doi.org/10.1016/j.watres.2016.11.049

Marusawa H, Ichikawa K, Narita N, Murakami H, Ito K, Tezuka T (2002) Hydroxyl radical as a strong electrophilic species. Bioorg Med Chem 10:2283–2290. https://doi.org/10.1016/S0968-0896(02)00048-2

Miralles-Cuevas S, Audino F, Oller I, Sánchez-Moreno R, Sánchez Pérez JA, Malato S (2014) Pharmaceuticals removal from natural water by nanofiltration combined with advanced tertiary treatments (solar photo-Fenton, photo-Fenton-like Fe(III)-EDDS complex and ozonation). Sep Purif Technol 122:515–522. https://doi.org/10.1016/j.seppur.2013.12.006

Moctezuma E, Leyva E, Aguilar CA, Luna RA, Montalvo C (2012) Photocatalytic degradation of paracetamol: intermediates and total reaction mechanism. J Hazard Mater 243:130–138. https://doi.org/10.1016/J.JHAZMAT.2012.10.010

Nogueira RFP, Oliveira MC, Paterlini WC (2005) Simple and fast spectrophotometric determination of H₂O₂ in photo-Fenton reactions using metavanadate. Talanta 66:86–91. https://doi.org/10.1016/J.TALANTA.2004.10.001

Nunes B, Antunes SC, Santos J, Martins L, Castro BB (2014) Toxic potential of paracetamol to freshwater organisms: a headache to environmental regulators? Ecotoxicol Environ Saf 107:178–185. https://doi.org/10.1016/J.ECOENV.2014.05.027

Odo EA, Britton DT, Gonfa GG, Harting M (2015) SAXS study of silicon nanocomposites. Int J Compos Mater 5:65–70

OECD (1999) Guidelines for Testing of Chemicals, Simulation Test-Aerobic Sewage Treatment 303a. Paris, France

Pamplona JH, Oba ET, da Silva TA, Ramos LP, Ramsdorf WA, Cestari MM, Oliveira Ribeiro CA, Zampronio AR, Silva de Assis HC (2011) Subchronic effects of dipyrone on the fish species Rhamdia quelen. Ecotoxicol Environ Saf 74:342–349. https://doi.org/10.1016/J.ECOENV.2010.09.010

Patlewicz G, Jeliazkova N, Safford RJ, Worth AP, Aleksiev B (2008) An evaluation of the implementation of the Cramer classification scheme in the Toxtree software. SAR QSAR Environ Res 19:495–524. https://doi.org/10.1080/10629360802083871

Ribeiro S, Torres T, Martins R, Santos MM (2015) Toxicity screening of diclofenac, propranolol, sertraline and simvastatin using danio rerio and paracentrotus lividus embryo bioassays. Ecotoxicol Environ Saf 114:67–74. https://doi.org/10.1016/J.ECOENV.2015.01.008

Riyajan S, Sakdapipanich JT, Tanaka Y (2003) Controlled degradation of cured natural rubber by encapsulated benzophenone as a photosensitizer. J Appl Polym Sci 90:297–305

Sakkas VA, Calza P, Islam MA, Medana C, Baiocchi C, Panagiotou K, Albanis T (2009) TiO$_2$/H$_2$O$_2$ mediated photocatalytic transformation of UV filter 4-methylbenzylidene camphor (4-MBC) in aqueous phase: statistical optimization and photoproduct analysis. Appl Catal B Environ 90:526–534

Sánchez C, Flores E, Barawi M, Clamagirand JM, Ares JR, Ferrer IJ (2016) Marcasite revisited: optical absorption gap at room temperature. Solid State Commun 230:20–24

Santiago-Morales J, Agüera A, Gómez M d M et al (2013) Transformation products and reaction kinetics in simulated solar light photocatalytic degradation of propranolol using Ce-doped TiO$_2$. Appl Catal B Environ 129:13–29. https://doi.org/10.1016/j.apcatb.2012.09.023

Santos LHMLM, Gros M, Rodriguez-Mozaz S, Delerue-Matos C, Pena A, Barceló D, Montenegro MCBSM (2013) Contribution of hospital effluents to the load of pharmaceuticals in urban wastewaters: identification of ecologically relevant pharmaceuticals. Sci Total Environ 461–462:302–316. https://doi.org/10.1016/j.scitotenv.2013.04.077

Sikorski KA (2014) Investigating the mechanism of phenol photooxidation by chromophoric dissolved organic matter. Doctoral dissertation, University of Maryland, College Park

Teófilo RF, Ferreira MMC (2006) Chemometrics II: spreadsheets for experimental design calculations, a tutorial. Quim Nova 29:338–350. https://doi.org/10.1590/S0100-40422006000200026

Teoh WY, Scott JA, Amal R (2012) Progress in heterogeneous photocatalysis: from classical radical chemistry to engineering nanomaterials and solar reactors. J Phys Chem Lett 3:629–639. https://doi.org/10.1021/jz3000646

Tobajas M, Belver C, Rodriguez JJ (2017) Degradation of emerging pollutants in water under solar irradiation using novel TiO$_2$-ZnO/clay nanoarchitectures. Chem Eng J 309:596–606. https://doi.org/10.1016/J.CEJ.2016.10.002

US EPA (2019) EPI Suite[TM]-Estimation Program Interface. https://www.epa.gov/tsca-screening-tools/epi-suitetm-estimation-program-interface. Accessed 3 Nov 2019

Wetchakun K, Wetchakun N, Sakulsermsuk S (2019) An overview of solar/visible light-driven heterogeneous photocatalysis for water purification: TiO$_2$- and ZnO-based photocatalysts used in suspension photoreactors. J Ind Eng Chem 71:19–49. https://doi.org/10.1016/J.JIEC.2018.11.025

Xu H, Cooper WJ, Jung J, Song W (2011) Photosensitized degradation of amoxicillin in natural organic matter isolate solutions. Water Res 45:632–638. https://doi.org/10.1016/j.watres.2010.08.024

Yan W, Yan L, Jing C (2019) Impact of doped metals on urea-derived g-C$_3$N$_4$ for photocatalytic degradation of antibiotics: structure, photoactivity and degradation mechanisms. Appl Catal B Environ 244:475–485

Yang L, Yu LE, Ray MB (2008) Degradation of paracetamol in aqueous solutions by TiO$_2$ photocatalysis. Water Res 42:3480–3488. https://doi.org/10.1016/J.WATRES.2008.04.023

Yang L, Yu LE, Ray MB (2009) Photocatalytic oxidation of paracetamol: dominant reactants, intermediates, and reaction mechanisms. Environ Sci Technol 43:460–465. https://doi.org/10.1021/es8020099

Zeghioud H, Assadi AA, Khellaf N, Djelal H, Amrane A, Rtimi S (2018) Reactive species monitoring and their contribution for removal of textile effluent with photocatalysis under UV and visible lights: dynamics and mechanism. J Photochem Photobiol A Chem 365:94–102. https://doi.org/10.1016/j.jphotochem.2018.07.031

Zeghioud H, Kamagate M, Coulibaly LS, Rtimi S, Assadi AA (2019) Photocatalytic degradation of binary and ternary mixtures of antibiotics: reactive species investigation in pilot scale. Chem Eng Res Des 144:300–309. https://doi.org/10.1016/j.cherd.2019.02.015

Zeghioud H, Nguyen-Tri P, Khezami L, Amrane A, Assadi AA (2020) Review on discharge plasma for water treatment: mechanism, reactor geometries, active species and combined processes. J Water Process Eng 38:101664

Zhi-Hong L (2013) A program for SAXS data processing and analysis. Chinese Phys C 37:108002